Thermal analysis of two-level wind power converter under symmetrical grid fault

Zhou, Dao; Blaabjerg, Frede

Published in:
Proceedings of the 39th Annual Conference of IEEE Industrial Electronics Society, IECON 2013

DOI (link to publication from Publisher):
10.1109/IECON.2013.6699422

Publication date:
2013

Thermal Analysis of Two-level Wind Power Converter under Symmetrical Grid Fault

Dao Zhou, Frede Blaabjerg

Department of Energy Technology
Aalborg University
Pontoppidanstraede 101, Aalborg, DK-9220, Denmark
zda@et.aau.dk, fbl@et.aau.dk

***Abstract*- In this paper, the case of symmetrical grid fault when using the multi-MW wind turbine of partial-scale and full-scale two-level power converter are designed and investigated. Firstly, the different operation behaviors of the relevant power converters under the voltage dip will be described and analyzed. Simulations of different configurations regarding the loss distribution and the junction temperature of the power device are presented in respect to the various voltage dips. It is concluded that for both systems the power loss will change dramatically during the Low-Voltage Ride Through (LVRT) condition as well as the junction temperature. For the full-scale wind turbine system, the most thermal stressed power device in the grid-side converter will appear at the grid voltage below 0.5 pu, and for the partial-scale wind turbine system, the most thermal stressed power device in the rotor-side converter will appear around 0.6 pu grid voltage.**

I. INTRODUCTION

Over the last two decades, the wind power industry has expanded greatly, and has become the fastest developing renewable energy technology in this period. In response to the steady growth of wind power demand, lower cost per kWh, increased power density and higher reliability of wind turbines are essential parameters [1]. Power electronic converters, as efficient interface between power grid and wind turbine generator, play a key role in wind power generation system. Although the power level of single wind turbine is even pushed up to 8 MW, the size power ratings of 1.5-3 MW are still the dominating on the commercial market [2].

As the wind power penetration to the power system in many countries increases, Transmission System Operators (TSOs) are challenged by the impacts to maintain reliability and stability of the power system. The new grid codes stipulate that wind farms should contribute to the power system voltage control in the case of abnormal operations of the network (e.g. voltage dips due to network faults). A presentation of the most critical requirement imposed by E.ON Netz is realized in [3], [4]. The behaviors under grid disturbance basically consist of two parts - Low Voltage Ride-Through (LVRT) capacity and Reactive Current Injection (RCI) capacity. The LVRT requirement is given in Fig. 1 for the network faults. Voltage drops within the area above the red line should not technically be disconnected. Even when the grid voltage drops to zero, the wind power plant must stay linked for 150 ms. During the grid fault, the active current can be reduced in order to fulfill the reactive power requirement. As described in Fig. 2, the proportional reactive current has to be injected with different grid voltage dips. If the voltage dip is above 0.5 pu, the wind power system should inject 1.0 pu over-excited reactive current to support and rebuild the grid voltage. Meanwhile, for the offshore wind farms, the grid voltage above 0.95 pu is regarded as the dead band boundary of RCI.

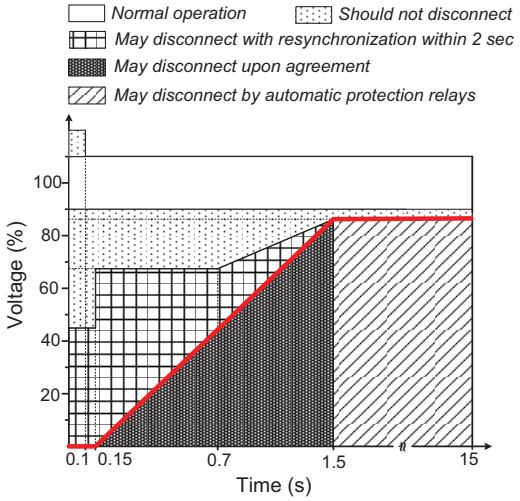

Fig. 1. Low-voltage ride through requirement in German grid code. [3]

A lot of work has been done on how to control the wind power converter to satisfy the grid codes during LVRT [5]-[7]. However, the loss and thermal performance under this condition is another important and interesting topic needed for further investigation [8], [9]. The scope of this paper is to investigate and simulate the power loss and the thermal cycling of the popular wind turbine systems undergoing the various balanced grid voltage dips. Firstly, the typical configurations and relevant grid codes will be introduced. Then, the operation behavior under LVRT for both systems will be described and investigated. Finally, the loss distribution and thermal analysis will be presented in respect to the various voltage dips.

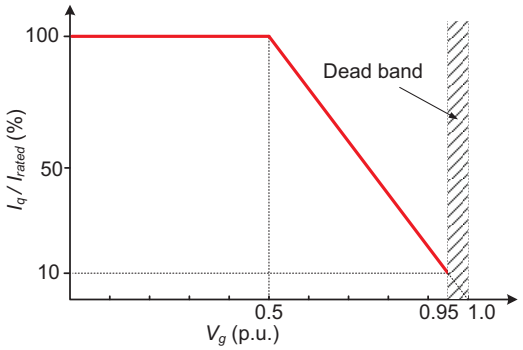

Fig. 2. Reactive current injection requirement of offshore wind turbines in German grid code. [3]

II. Operation Behavior under Voltage Dips

A 2 MW wind turbine system is selected for the case studies. The relevant parameters of a Doubly-Fed Induction Generator (DFIG) based and a Permanent Magnet Synchronous Generator (PMSG) based wind turbine system are summarized in Table I [10]. In order to facilitate the investigation and demonstration of the wind power converter operation behavior under LVRT, three-phase symmetrical grid dip is firstly taken into consideration.

TABLE I
PARAMETERS FOR 2 MW DFIG AND PMSG WIND TURBINE SYSTEMS

	DFIG system	PMSG system
Rated power of converter P_g [kW]	330	2000
Rated grid phase voltage U_{gm} [V]	564	564
DC-link voltage U_{dc} [V]	1050	1100
Filter inductance L_g [mH]	0.5	0.15
Stator inductance L_s [mH]	2.94	0.276
Magnetizing inductance L_m [mH]	2.91	
Switching frequency of power device f_s [kHz]	2	2
Power device in each grid-side converter arm	1 kA/1.7 kV single	1 kA/1.7 kV four in parallel
Power device in each generator-side converter arm	1 kA/1.7 kV two in parallel	1 kA/1.7 kV four in parallel

A. PMSG system

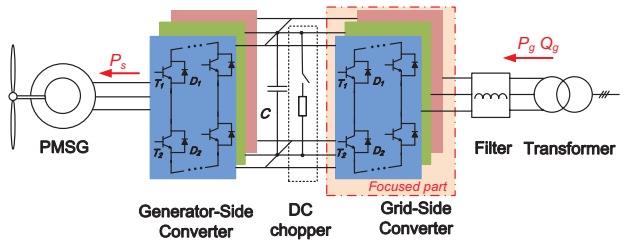

Fig. 3. PMSG-based full-scale wind power converter.

Due to the back-to-back power converter fully decouple between the grid and the PMSG, it is known that the full-scale wind power converter has a better and more reliable LVRT capability. As shown in Fig. 3, because the grid-side converter is directly connected to the grid and plays a key role to fulfill the stricter standard during grid faults, the discussions will mainly focus on this part of the generation system at this stage.

Fig. 4 indicates the active power P_g and reactive power Q_g delivered by the grid-side converter under various three-phase balanced grid voltage dips. According to the description of the RCI in Fig. 2, if the grid voltage dip is more than 0.5 pu, the reactive power reference will linearly increase proportional to the grid voltage; if the grid voltage dip is less than 0.5 pu, it will decrease rapidly mainly due to the less RCI demand. Moreover, the active power will stay zero if the grid voltage dip is below 0.5 pu. The active power for the grid-side converter will normally follow the maximum power point tracking as soon as possible for the wind turbine. The conditions of 12 m/s (2 MW), 10.1 m/s (1.29 MW) and 5.9 m/s (0.26 MW) are indicated in Fig. 4, respectively. Because of the relatively smaller active power reference at lower wind speed, the grid-side converter has an additional flexibility of the reactive current output capability. Consequently, it is noted that at lower wind speed, the smaller effect is made on the active power reference.

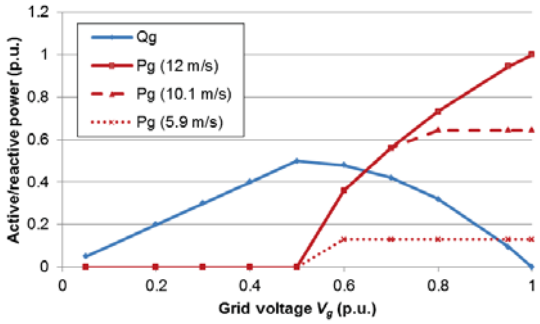

Fig. 4. Active and reactive power under various balanced grid voltage dips and wind speeds for the PMSG system.

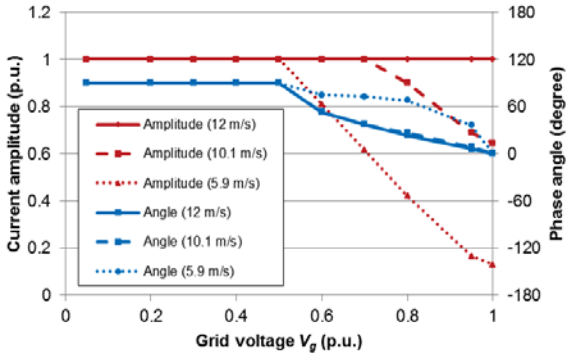

Fig. 5. Amplitude and phase angle of the loading current during balanced LVRT for the PMSG system.

As the output current amplitude and the phase angle are quite relevant to the power loss as well as the thermal performance of the power semiconductors, both of them are shown in Fig. 5 at the wind speeds of 12 m/s, 10.1 m/s and 5.9 m/s, respectively, where the amplitude of the loading current

can be derived in terms of the active current and reactive current. If the wind speed is at 12 m/s, the amplitude of the current will remain 1.0 pu during all kinds of various grid voltage dips; while if the wind speed is at 5.9 m/s, the current will dramatically increase with higher level of voltage drop, because the reactive current component dominates the current amplitude. Meanwhile, when the voltage dip is lower than 0.5 pu, the phase angle between the loading current and grid voltage at all wind speeds begins to change remarkably.

B. DFIG system

As shown in Fig. 6, although both the grid-side converter and rotor-side converter are theoretically able to support the RCI during the grid voltage dips, due to stator and rotor winding turns ratio as well as the de-rating design, it is a better idea to compensate the reactive power from the rotor-side converter. As a result, the discussions will only focus on this part for the generation system.

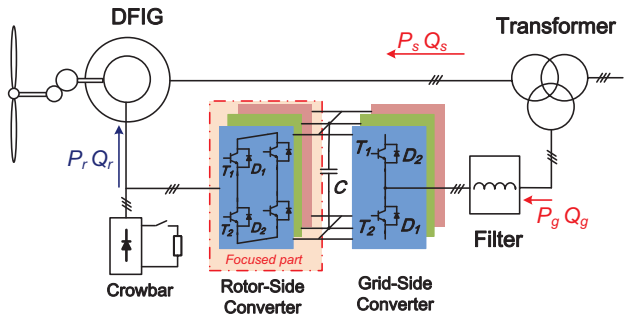

Fig. 6. DFIG-based partial-scale wind power converter.

As the stator of the DFIG is directly linked to the grid, the sudden grid voltage drop will introduce a natural flux in the stator winding, which may produce large transient current in the rotor-side and may destroy the rotor-side converter [7]. This dynamical situation may be the most critical period. However, for simplicity it is assumed that the initial stator flux is consistent with the various voltage dips, which theoretically omits the transient situation.

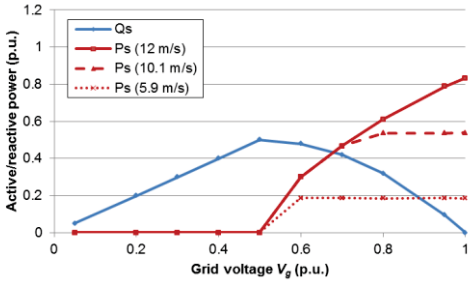

Fig. 7. Active and reactive power under various balanced grid voltage dips for the DFIG system.

Fig. 7 indicates the active power P_s and reactive power Q_s delivered by the stator-side under various balanced grid voltage dips of three-phase. The reactive power reference is exactly the same as the PMSG system, but the active power reference will be slightly different than the PMSG system due to the doubly-fed mechanism of the system.

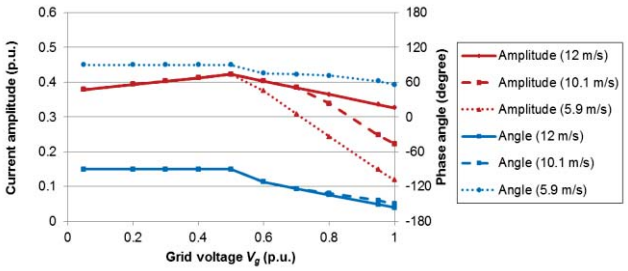

Fig. 8. Amplitude and phase angle of the loading current during balanced LVRT for the DFIG system.

According to the steady-state equivalent DFIG model, if the stator active power and reactive power in d-axis and q-axis is introduced [11], the rotor current i_r' and the rotor voltage u_r' (referred to the stator-side) can be expressed as,

$$\begin{cases} i_{rd}' = -\dfrac{2}{3}\dfrac{X_s}{X_m}\dfrac{P_s}{U_{sd}} \\ i_{rq}' = -\dfrac{U_{sd}}{X_m} + \dfrac{2}{3}\dfrac{X_s}{X_m}\dfrac{Q_s}{U_{sd}} \end{cases} \tag{1}$$

$$\begin{cases} u_{rd}' = s\left(\dfrac{X_r}{X_m}U_{sd} - \dfrac{2}{3}\dfrac{\sigma X_r X_s}{X_m}\dfrac{Q_s}{U_{sd}}\right) \\ u_{rq}' = -\dfrac{2}{3}s\dfrac{\sigma X_r X_s}{X_m}\dfrac{P_s}{U_{sd}} \end{cases} \tag{2}$$

where X_s, X_r and X_m denotes the stator, rotor and magnetizing reactance at 50 Hz, s denotes the rotor slip value, σ denotes the leakage factor of the induction generator, U_{sd} denotes the peak stator phase voltage of the induction generator.

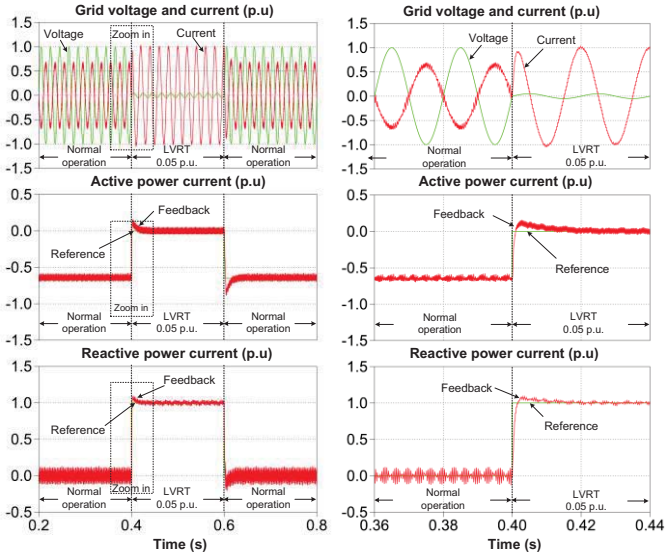

Fig. 9. Simulation results of the PMSG system during LVRT period at v_w=10.1 m/s. (a) Overview; (b) Zoom of transient period.

The amplitude and phase angle of the rotor-side current during balanced LVRT is shown in Fig. 8, where the wind speeds of 12 m/s, 10.1 m/s and 5.9 m/s are independently evaluated. It can be seen that the maximum current amplitude appears at 0.5 pu grid voltage, and the amplitude of the rotor-side current will decrease dramatically if the grid voltage dip is less than 0.5 pu for all wind speeds. For the phase angle of

the rotor current and the rotor voltage, it will almost be reverse between the sub-synchronous mode and super-synchronous mode because of the change of the active power flow.

Simulation validation of the loading current characteristic can be realized based on PLECS blockset in Simulink [12]. The simulation settings correspond to the values given in Table I. Consider that an extreme voltage dip 0.05 pu occurs at the time of 0.4 second, the simulation results of the PMSG system during LVRT period is shown in Fig. 9. During the transient period, it is noted that the active power and reactive power could track the reference signal well. The amplitude of the loading current increase from almost 0.6 pu to 1.0 pu, and phase angle change from 0º (releasing active power) to 90º (injecting the reactive power). It indicates the remarkably different current distribution share between the IGBT and the diode in the same power module, which implies that the power loss breakdown between the IGBT and the diode will also be significantly affected.

For the DFIG system, the simulation validation for normal operation and LVRT condition at the steady-state is shown in Fig. 10(a) and Fig. 10(b), respectively, where the voltage and the current of the stator-side and rotor-side of the induction generator are analyzed. According to the grid codes requirement, the stator-side will reduce the active power output and supply the over-excited reactive power to support the grid voltage recovery during LVRT, which is shown in the upper of Fig. 10. In the lower Fig. 10, the induced voltage and current of rotor-side also changes as well as the phase angle between them. Moreover, it is noted that the amplitude of rotor current becomes higher during the LVRT operation.

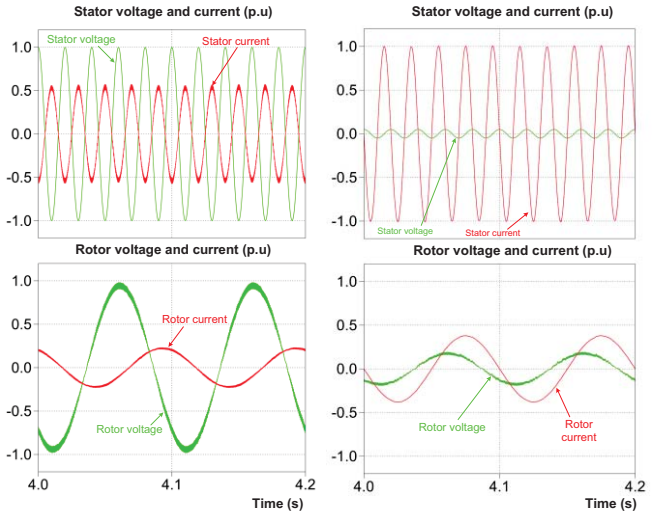

(a) (b)

Fig. 10. Simulation results of the DFIG system at v_w=10.1 m/s. (a) Normal operation; (b) LVRT=0.05 pu.

III. Loss Distribution During LVRT

The power loss model, consisting of the conduction losses and the switching losses, can be referred to [10]. Based on the on-state voltage drop and switching energy against the loading current and the DC-link voltage provided by the manufacturers, the conduction losses and the switching losses are accumulated by every switching cycle within one fundamental frequency. The simulation of the power loss has been realized according to the PLECS blockset in Simulink.

The loss comparison of each power semiconductor in the power converter arm under normal and LVRT operation can be seen in Fig. 11, where the case studies for the PMSG system and the DFIG system are shown in Fig. 11(a) and Fig. 11(b), respectively. In Fig. 11(a), for the grid-side converter the power loss distribution for three normal operations at different wind speeds and one LVRT condition is listed. It is noted that the power loss consistently increases with larger wind speed at normal operation, and the IGBT dominates the power dissipation due to the direction of the power flow. Moreover, it is worth to note that in the condition of the LVRT, the loss distribution will be quite different compared with the normal operation at 10.1 m/s wind speed, where the diode and IGBT will both have higher power dissipation mainly due to the higher amplitude of loading current.

In Fig. 11(b), for the rotor-side converter in the DFIG system, it is noted that the power loss between the IGBT and the diode will be more unequal during the LVRT operation, and it is also the LVRT operation that consumes the most power dissipation.

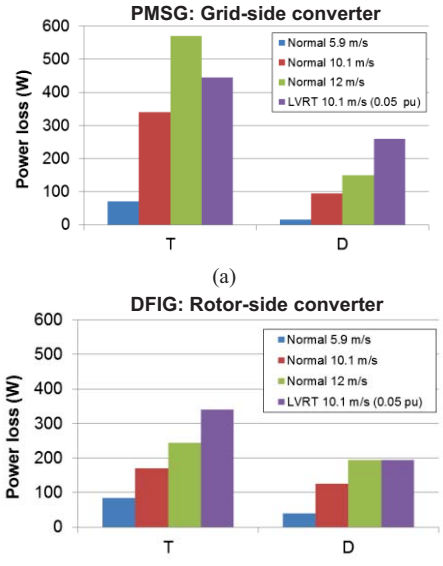

(a)

(b)

Fig. 11. Loss comparison of each power semiconductor inside power converter arm under normal and LVRT situation. (a) Grid-side converter in the PMSG system; (b) Rotor-side converter in the DFIG system. Note: *T* stands for the transistor and *D* stands for the diode.

IV. Thermal Distribution

As shown in Fig. 12, a one-dimensional thermal model of a single IGBT and a freewheeling diode shares the same idea as discussed in [13]. With the aid of the power loss as shown in Fig. 11, the junction temperature can again be simulated using the PLECS-software.

For the PMSG system, the junction temperature comparison in the grid-side converter illustrated in Fig. 3 between normal

operation and LVRT is shown in Fig. 13, where the wind speed is assumed 10.1 m/s. It can be seen that the LVRT condition will induce a higher junction temperature both in the IGBT and the diode. Although the mean junction temperature of the IGBT and the diode becomes more equal, the junction temperature fluctuation of them is higher.

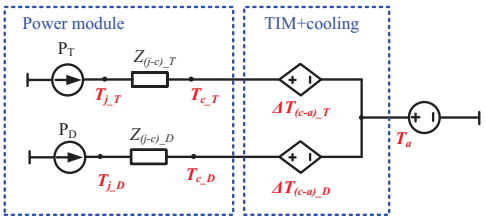

Fig. 12. Thermal model of the power switching device.

Based on the well-known Coffin-Manson lifetime models, the mean junction temperature and the junction temperature fluctuation of the power semiconductor are the most important two indicators. Hence, it is interesting to investigate the thermal excursion of the power device under various grid voltage dips as shown in Fig. 14, where the wind speeds at 12 m/s, 10.1 m/s and 5.9 m/s are studied, respectively. It can be seen that both the mean junction temperature and the junction temperature fluctuation of the power devices perform smoothly if the symmetrical voltage dip is above 0.5 pu at all kinds of the wind speeds due to the completely reactive current injection. However, the mean junction temperature and the junction temperature fluctuation at all wind speeds start to change dramatically if the grid voltage dip is below 0.5 pu.

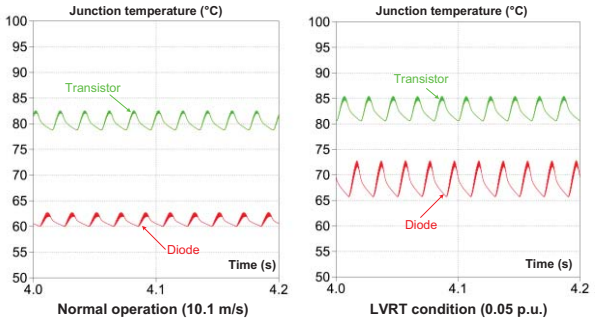

(a) (b)

Fig. 13. Junction temperature in normal operation vs LVRT in grid-side converter for the PMSG system at v_w=10.1 m/s.
(a) Normal operation; (b) LVRT condition (0.05 pu).

It can be seen that the most stressed power devices appear in case of the wind speed 12 m/s from either the mean junction temperature or the junction temperature fluctuation point of view. For the mean junction temperature, the IGBT is more heated than the diode at all various grid dips. Moreover, with the increase of the grid dip level, the power loss switches from the IGBT to the diode. As a result, the IGBT has lower mean junction temperature, while the mean junction temperature of the diode has larger value. The IGBT and the diode reach a more equal distribution if the grid voltage dip is higher than 0.5 pu. Furthermore, it is found that the highest junction temperature fluctuation changes from the IGBT to the diode around grid voltage 0.6 pu.

In case of the wind speed at 10.1 m/s, from the diode point of view, the mean junction temperature and the junction temperature fluctuation keep increasing with the higher level of voltage dip until the dip value is 0.5 pu. However, it can be found that the IGBT will reach a peak value for both the mean junction temperature and the junction temperature fluctuation around 0.7 pu grid voltage, due to the quick changing power angle and the fast growing switching loss. In case of the wind speed at 5.9 m/s, the most stressed situation appears if the grid voltage is below 0.5 pu for both the IGBT and the diode.

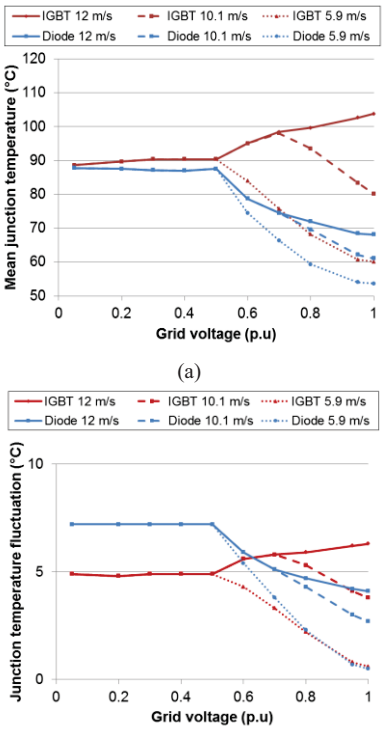

(a)

(b)

Fig. 14. Junction temperature under various symmetrical grid dips in the grid-side converter for the PMSG system.
(a) Mean junction temperature value vs grid voltage;
(b) Junction temperature fluctuation vs grid voltage.

For the DFIG system, the comparison of the junction temperature in the rotor-side converter illustrated in Fig. 6 between normal operation and LVRT is shown in Fig. 15. It can be seen that the LVRT condition will induce a higher junction temperature for both the IGBT and the diode, which is consistent with the power loss analysis in Fig. 11(b).

The simulated mean junction temperature and the junction temperature fluctuation of each switching device in the rotor-side converter in relation to the grid voltage are shown in Fig. 16(a) and Fig. 16(b), respectively. Both the mean junction temperature and the junction temperature fluctuation vary a little bit if the symmetrical grid dip is above 0.5 pu, while they change dramatically if the grid voltage dip is below 0.5 pu. It is noted that the most stressed power devices appear in case of the wind speed 12 m/s. The highest mean junction temperature and the junction temperature fluctuation for the IGBT appear at 0.5 pu, but from the diode point of view, they become highest around 0.7 pu. In case of the wind speed 5.9 m/s, the

most stressed power devices appear at 0.5 pu. Moreover, if the grid voltage is below 0.5 pu, although the mean junction temperature shows the similar performance as other wind speeds, the junction temperature fluctuation becomes less stressed due to the higher fundamental frequency of the loading current.

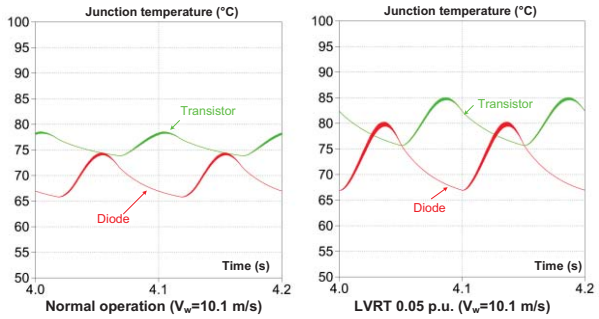

(a) (b)

Fig. 15. Junction temperature in normal operation vs LVRT in the rotor-side converter for the DFIG system at v_w=10.1 m/s.
(a) Normal operation; (b) LVRT condition (0.05 pu).

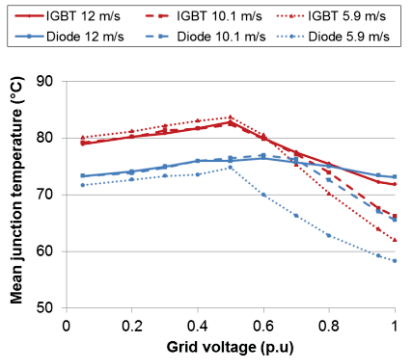

(a)

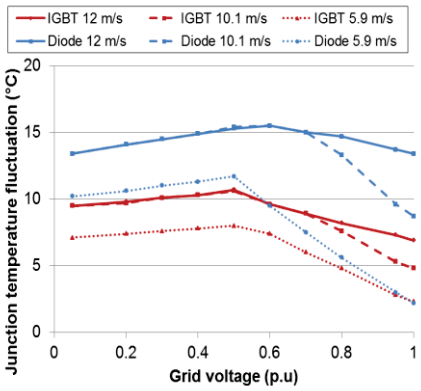

(b)

Fig. 16. Junction temperature under various symmetrical grid dips in rotor-side converter for the DFIG system.
(a) Mean junction temperature value vs grid voltage;
(b) Junction temperature fluctuation vs grid voltage.

V. CONCLUSION

In this paper, the operation behaviors of the popular 2 MW two-level power converter wind turbine configurations (partial-scale and full-scale power converter) are evaluated at different wind speeds. The power losses and the thermal cycling in respect to various grid voltage dips are investigated and simulated.

For the PMSG system, according to the German grid codes, the loading current in the grid-side converter will change dramatically if the grid dips emerges. However, the loading current will keep unchanged, if the grid voltage is below 0.5 pu. Moreover, the most loading power semiconductor will switch from the IGBT to the diode with a higher level of grid dip from the junction temperature fluctuation point of view, and the most thermal stressed power semiconductor will appear at the grid voltage below 0.5 pu.

For the DFIG system, the current in the rotor-side converter will increase dramatically, if the grid dip begins, and the maximum current appear at grid voltage 0.5 pu. Furthermore, from the junction temperature fluctuation point of view, the most stressed power semiconductor will remain the diode with different levels of grid dips, and the most thermal stressed power device will appear at the grid voltage around 0.6 pu.

References

[1] F. Blaabjerg, Z. Chen, S. B. Kjaer, "Power electronics as efficient interface in dispersed power generation systems," *IEEE Trans. on Power Electronics*, vol. 19, no. 5, pp. 1184- 1194, Sep. 2004.

[2] M. Liserre, R. Cardenas, M. Molinas, J. Rodriguez, "Overview of multi-MW wind turbines and wind parks," *IEEE Trans. on Industrial Electronics*, vol. 58, no. 4, pp. 1081-1095, Apr. 2011.

[3] E.ON-Netz. *Requirements for offshore grid connections*, Apr. 2008.

[4] M. Tsili, S. Papathanassiou, "A review of grid code technical requirements for wind farms," *IET on Renewable Power Generation*, vol. 3, no. 3, pp. 308-332, Sep. 2009.

[5] D. Xiang, L. Ran, P. Tavner, S. Yang, "Control of a doubly fed induction generator in a wind turbine during grid fault ride-through," *IEEE Trans. on Energy Conversion*, vol. 21, no. 3, pp. 652-662, Sep. 2006.

[6] J. Lopez, E. Gubia, E. Olea, J. Ruiz, L. Marroyo, "Ride through of wind turbines with doubly fed induction generator under symmetrical voltage dips," *IEEE Trans. on Industrial Electronics*, vol. 56, no. 10, pp. 4246-4254, Oct. 2009.

[7] F. Lima, A. Luna, P. Rodriguez, E. Watanabe, F. Blaabjerg, "Rotor voltage dynamics in the doubly fed induction generator during grid faults," *IEEE Trans. on Power Electronics*, vol. 25, no. 1, pp. 118-130, Jan. 2010.

[8] K. Ma, F. Blaabjerg, M. Liserre, "Thermal analysis of multilevel grid-side converters for 10-MW wind turbines under low-voltage ride through," *IEEE Trans. on Industry Applications*, vol. 49, no. 2, pp. 909-921, Mar. 2013.

[9] K. Ma, M. Liserre, F. Blaabjerg, "Reactive power influence on the thermal cycling of multi-MW wind power inverter," *IEEE Trans. on Industry Applications*, vol. 49, no. 2, pp. 922-930, Mar. 2013.

[10] D. Zhou, F. Blaabjerg, M. Lau, M. Tonnes, "Thermal analysis of multi-MW two-level wind power converter," *in Proc. of IECON 2012,* pp. 5862-5868, 2012.

[11] D. Zhou, F. Blaabjerg, M. Lau, M. Tonnes, "Thermal behavior optimization in multi-MW wind power converter by reactive power circulation," *IEEE Trans. on Industry Applications*, to be published.

[12] User manual of PLECS blockset version 3.2.7 March 2011. (Available: http://www.plexim.com/files/plecsmanual.pdf

[13] D. Zhou, F. Blaabjerg, M. Lau, M. Tonnes, "Thermal profile analysis of doubly-fed induction generator based wind power converter with air and liquid cooling methods," *in Proc. of EPE 2013*, to be published.